Published in Applied Physics Letters 79, 4271-4273, 2001
which should be used for any reference to this work

Long-wavelength ($\lambda \approx 16\ \mu$m), room-temperature, single-frequency quantum-cascade lasers based on a bound-to-continuum transition

Michel Rochat,[a] Daniel Hofstetter, Mattias Beck,[b] and Jérôme Faist[c]
Institute of Physics, University of Neuchâtel, CH-2000 Neuchâtel, Switzerland

Room-temperature operation of long-wavelength, Fabry–Perot and single-mode quantum-cascade lasers at $\lambda \approx 16\ \mu$m is reported. Multimode emission with pulsed peak power up to 400 mW at -40 °C and 220 mW at 30 °C is demonstrated. Single-mode emission up to 60 mW peak power has been achieved at 30 °C.

The Quantum Cascade (QC) laser[1] is a unipolar semiconductor laser that has demonstrated high performance in pulsed operation in the mid-infrared wavelength range (4–12 μm). There has been a large effort to develop such devices for even longer wavelengths. These sources would be especially valuable for the detection of large organic hydrocarbon molecules like the BTX compounds in the 12–16 μm region or for radio-astronomy as local oscillators in heterodyne detectors.

Devices designed using the so-called three quantum well active region were demonstrated with an operation wavelength up to $\lambda \approx 13\ \mu$m.[2] However, these devices exhibited fairly limited performances with a maximum operating temperature of $T_{max}=175$ K. Devices based on chirped superlattice active regions demonstrated operation at much longer wavelengths, reaching 17, 19, 21 and finally up to $\lambda \approx 24\ \mu$m.[3–6] However, these structures were limited to operation temperatures below 200–240 K.

When trying to design long-wavelength quantum-cascade lasers, for photon energies larger than the reststrahlen band, population inversion is more difficult to achieve as the upper state lifetime decreases with emitted photon energy, due to the dependence of the optical phonon scattering rate on exchanged wave vector. The lower state lifetime, on the other hand, remains practically unchanged. For this reason, and especially if high temperature operation is seeked, long-wavelength QC lasers must be designed with extremely short lower state lifetimes. Transport in wide minibands, compared with the optical phonon energy, provides efficient lower state extraction mechanism. As the ''bound-to-continuum'' design combines the fast miniband extraction from the lower state with the efficient resonant tunneling injection into the upper state,[7] this approach is very well suited for long wavelength lasers.

As shown schematically in Fig. 1, the active region of our structure spans the whole period and consists of a chirped superlattice presenting a tilted lower miniband whose width is maximum in the center and decreases on both sides close to the injection barriers. The upper state is created in the first minigap by a small well adjacent to the injection barrier. Its wave function has a maximum close to the injection barrier and decreases smoothly in the active region. This upper state is well separated from the higher-lying states of the superlattice, lying in its first minigap and therefore does not need to be confined by separating the structure into an active region and an injection/relaxation region. The computed upper state lifetime $\tau_{up}=0.68$ ps, is longer than the one $\tau_{up}=0.55$ ps computed for a chirped superlattice emitting at $\lambda = 17\ \mu$m.[3] This is due to the slightly diagonal nature of the laser transition which leads to a reduced overlap of the upper and lower state wave functions and to a further improved ratio of upper to lower state lifetimes.

In a bound-to-continuum design, the oscillator strength is not concentrated in a single transition, as is the case for a symmetric superlattice but is instead ''spread'' over two or three states spanning an energy range of $\approx$20 meV.[7] This is in principle a disadvantage of this design as the peak gain is, in a simplified atomistic picture, inversely proportional to the linewidth of the transition. However, for devices based on multiquantum well active region and optimized for room temperature operation, the intersubband transitions are anyway collision broadened to a width of 15–25 meV. Due to the reduced overlap between upper and lower laser state

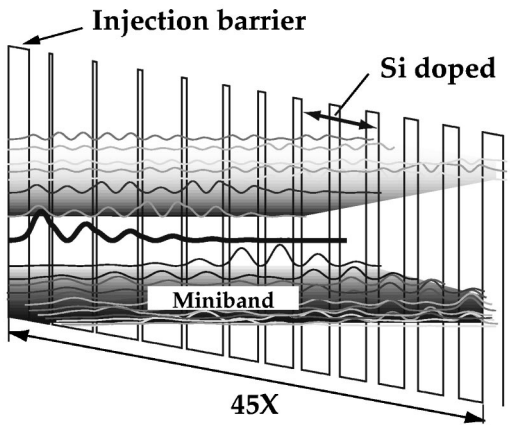

FIG. 1. Schematic conduction band diagram of one stage of the structure under an applied electric field of 2.1×10^4 V cm^{-1}. The moduli squared of the relevant wave functions are shown. The layer sequence of one period of structure, in nanometers, left to right and starting from the injection barrier is **3.3**/3.2/**0.5**/6.5/**0.6**/6.6/**0.7**/6.3/**0.8**/5.8/**1.0**/4.6/**1.2**/4.4/**1.4**/4.4/**1.7**/4.2/**2.0**/4.1/**2.2**/4.0/**2.5**/3.8/ where $In_{0.52}Al_{0.48}As$ layers are in bold, $In_{0.53}Ga_{0.47}As$ in Roman and underlined numbers correspond to the doped region (Si, 3×10^{17} cm^{-3}).

[a]Electronic mail: Michel.Rochat@unine.ch
[b]Also with Alpes Lasers, www.alpeslasers.com
[c]Electronic mail: Jerome.Faist@unine.ch

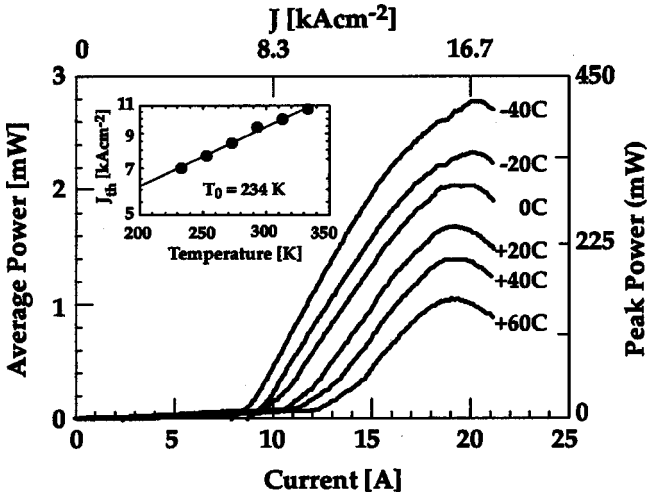

FIG. 2. Optical output power vs injected current in pulsed mode with a duty cycle of 0.67% at various temperatures for a device with a Fabry–Perot cavity. Threshold current density as a function of temperature is shown in the inset.

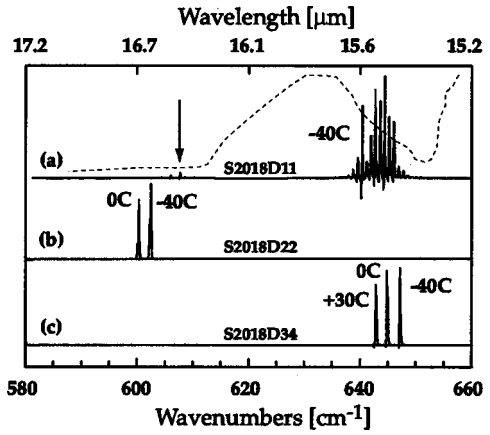

FIG. 3. (a) Spectral emission from a device with a Fabry–Perot waveguide; (b) with a grating designed to force the lasing mode at $\lambda \approx 16.5\ \mu$m, and (c) with a grating designed for $\lambda \approx 15.5\ \mu$m.

wave function, the equivalent dipole matrix element of the laser transition (averaged over the transitions to the two upper states of the lower miniband) is $z = 4.0$ nm, lower than the value obtained for a chirped superlattice sample $z = 5.0$ nm. The structure was grown by molecular beam epitaxy using InGaAs and AlInAs alloys lattice matched on top of a very low *n*-doped InP substrate (Si, $n = 1 \times 10^{17}\ \mathrm{cm}^{-3}$) and consist of a 45 period active region embedded in an optical waveguide. In contrast to the previous works, where extensive use of surface plasmon waveguide was made,[8] we chose a waveguide design which relies on dielectric confinement.[9] It consists of two low doped (Si, $n = 6 \times 10^{16}\ \mathrm{cm}^{-3}$) InGaAs guiding layers, respectively, 600 and 1750 nm thick, grown below and above the active region. The computed waveguide absorption at $\lambda = 16\ \mu$m caused by free carriers is $\alpha = 30\ \mathrm{cm}^{-1}$, neglecting the contributions from multiphonon processes. Electrical injection in the structure is obtained laterally through a heavily doped Si, $n = 1 \times 10^{18}\ \mathrm{cm}^{-3}$) 600-nm-thick InGaAs *n*-doped contact layer. The devices were processed in 50- to 75-μm wide mesa ridge waveguides using wet chemical etching and a hard baked resist layer for passivation. Contacts were then provided by a Ti/Au metallization (10/400 nm) on the top edges of the waveguides. Back contacting (Ge/Au/Ag/Au, 12/27/50/100 nm) the thinned substrate ended the processing. The samples were then soldered with indium on a copper heat sink and mounted on a Peltier cooler inside an aluminum box with a ZnSe window. The electrical power was provided to the lasers with a commercial pulse generator (Alpes Lasers, TPG 128 pulser, and a LDD 100 power supply) delivering 25- to 50-ns-long current pulses at a variable repetition rate up to 5 MHz. The optical output power was directly measured by a calibrated thermopile. Spectral measurements were performed by a Fourier transform infrared spectrometer in rapid scan mode and a liquid-nitrogen cooled MCT detector.

Typical $L-I$ curves from a 75-μm-wide and 1.6 mm-long Fabry–Perot device are shown in Fig. 2 for temperatures ranging from -40 up to 60 °C. The sample is driven with 25-ns-long current pulses and a duty cycle of 0.67%. At -40 °C the threshold current density is 6.7 kA cm^{-2} with a maximum average output power 2.8 mW leading to a peak power of more than 400 mW. At 60 °C, the threshold current density is 10 kA cm^{-2} and the maximum output power is measured to be more than 1 mW. At -40 °C, we achieved a maximum output power of 5.5 mW with 3% duty cycle and 1.2 mW at 60 °C (1.5% duty). At -40 °C, the highest achieved duty cycle was 9.6%. A fit to the threshold current density dependence with temperature (inset of Fig. 2) using the usual expression $J = J_0 \exp(T/T_0)$ yields a value of $T_0 = 234$ K. The emission spectrum of this multimode device, [Fig. 3(a)] consists mainly of modes around 644 cm^{-1} ($\lambda \approx 15.5\ \mu$m). However weaker features around 607 cm^{-1} ($\lambda \approx 16.5\ \mu$m) are also visible (see arrow). They show that the gain curve of the device is broad (more than 40 cm^{-1}) and suggest the possibility to force the device to lase in this spectral region. Dotted line above the spectra represents the two-phonon absorption of InP on a linear arbitrary scale.[10] We clearly observe a correlation between the minima of the two phonon absorption and the lasing frequencies of our device. To demonstrate the possibility for our structure to lase in two spectrally distant regions, we have processed two series of samples with gratings etched into the waveguide[11] with periods designed to force waveguide modes at $\lambda \approx 16.5\ \mu$m and $\lambda \approx 15.5\ \mu$m. An effective refractive index $n_{\mathrm{eff}} = 3.001$ was used to compute the gratings periodicities. Figure 3(b) displays the spectral measurements for 1.5-mm-long and 50-μm-wide sample S2018D22 with a grating period designed for the $\lambda \approx 16.5\ \mu$m region. At -40 °C, the threshold current density is 7.0 kA cm^{-2}. Up to an average power of $P = 0.2$ mW, the emission is single frequency at 602 cm^{-1} ($\lambda \approx 16.6\ \mu$m). However, as the driving current is increased further, side modes around the main peak at 602 cm^{-1} build up and the peak at 647 cm^{-1} reappears. A maximum (multimode) output power of 2.1 mW has been achieved. With increasing temperature, the peak redshifts from 602 down to 600 cm^{-1} ($\lambda \approx 16.7\ \mu$m) at 0 °C. Results from sample S2018D34, with a shorter grating period, are shown in Fig. 3(c). At -40 °C, the emission peak is centered at 647 cm^{-1} with a threshold current density of 6.1 kA cm^{-1}. Furthermore, the emission is single mode up to an injected current density of 8.7 kA cm^{-1} with an output power of $P = 0.85$ mW (64 mW peak) (inset of Fig. 4). Increasing the

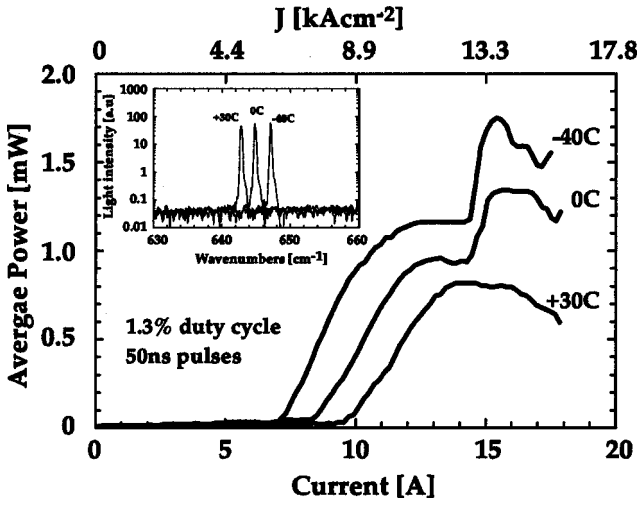

FIG. 4. $L-I$ curves with increasing temperature are shown for sample S2018D34. The sample is processed into a 2.250-mm-long and 50-μm-wide waveguide. Inset is the spectral emission from sample S2018D34 plotted on a logarithmic scale, showing that the emission is single mode with a maximum output power 0.85 mW at -40 °C.

injection current density up to 11 kA cm^{-1} leads to a saturation of the output power at 1.2 mW. At this current density, the emission consists of a single frequency peak around 647 cm^{-1} and a small feature at 638 cm^{-1}. Increasing further the current, strongly increases the output power until a maximum of 1.75 mW is reached. At this stage, the emission spectra is multimode and centered at 646 cm^{-1}. At $+30$ °C, the emission is single mode up to the device's maximum operation capabilities with an average output power of $P = 0.8$ mW at 1.3% duty cycle. The peak is redshifted down to 642 cm^{-1} leading to a temperature tuning $\Delta\upsilon/\Delta T$ of -0.07 cm^{-1}K^{-1}.

Measurements done on 750-μm-long structures show that the spectral emission is not single mode and suggest the need for a much stronger grating in order to achieve single-mode laser operation for such short cavities. Similarly, higher power output in single-mode operation should be achieved in the 600 cm^{-1} region with deeper etched gratings.

In conclusion, long wavelength 16 μm quantum cascade lasers are demonstrated at room temperature with high peak output power using a bound-to-continuum structure design. Peak multimode output power of more than 400 mW been achieved at -40 °C. At 60 °C, the output power was still more than 150 mW peak. We have also demonstrated the wide tuning possibilities of the bound-to-continuum gain material as we are able to force our devices to lase either at 15.5 or at 16.7 μm with the same structure by varying the period of an etched grating into the waveguides. These are the longest wavelengths reported for a quantum cascade laser at non-cryogenic temperatures. These lasers could enable the development of portable BTX sensors based on optical techniques.

This work was supported in part by the Swiss National Science Foundation and by European project Supersmile.

[1] J. Faist, F. Capasso, C. Sirtori, D. Sivco, and A. Cho, "Quantum cascade lasers," in *Intersubband transitions in quantum wells: Physics and device applications, II*, edited by H. Liu and F. Capasso (Academic, New York, 2000), Vol. 66, Chap. 1, pp. 1–83.
[2] C. Gmachl, F. Capasso, A. Tredicucci, D. Sivco, A. Hutchinson, and A. Cho, Electron. Lett. **34**, 1103 (1998).
[3] A. Tredicucci, C. Gmachl, F. Capasso, D. Sivco, A. Hutchinson, and A. Cho, Appl. Phys. Lett. **74**, 638 (1999).
[4] A. Tredicucci, C. Gmachl, F. Capasso, A. Hutchinson, D. Sivco, and A. Cho, Appl. Phys. Lett. **76**, 2164 (2000).
[5] A. Tredicucci, C. Gmachl, M. Wanke, F. Capasso, A. Hutchinson, D. Sivco, S. Chu, and A. Cho, Appl. Phys. Lett. **77**, 2286 (2000).
[6] R. Colombelli, F. Capasso, C. Gmachl, A. Hutchinson, D. Sivco, A. Tredicucci, M. Wanke, A. Sergent, and A. Cho, Appl. Phys. Lett. **78**, 2620 (2001).
[7] J. Faist, M. Beck, T. Aellen, and E. Gini, Appl. Phys. Lett. **78**, 147 (2001).
[8] C. Sirtori, C. Gmachl, F. Capasso, J. Faist, D. Sivco, A. Hutchinson, and A. Cho, Opt. Lett. **23**, 1366 (1998).
[9] D. Hofstetter, T. Aellen, M. Beck, and J. Faist, IEEE Photonics Technol. Lett. **12**, 1610 (2000).
[10] E. Koteles and W. Datars, Solid State Commun. **19**, 221 (1976).
[11] D. Hofstetter, J. Faist, M. Beck, A. Müller, and U. Oesterle, Appl. Phys. Lett. **75**, 665 (1999).